JGR Oceans

RESEARCH ARTICLE
10.1029/2019JC015554

Arctic Ocean Surface Energy Flux and the Cold Halocline in Future Climate Projections

Enrico P. Metzner[1], Marc Salzmann[1], and Rüdiger Gerdes[2,3]

[1]Institute for Meteorology, Universität Leipzig, Leipzig, Germany, [2]Alfred Wegener Institute, Helmholtz Centre for Polar and Marine Research, Bremerhaven, Germany, [3]Physics and Earth Sciences, Jacobs University, Bremen, Germany

Key Points:
- Climate models show increasing Arctic Ocean energy release through the surface in winter and spring
- Sharp temperature gradients below the surface mixed layer facilitate this increased energy release
- Warm water from below increasingly reaches the surface mixed layer in future climate projections

Supporting Information:
- Supporting Information S1

Correspondence to:
M. Salzmann,
marc.salzmann@uni-leipzig.de

Citation:
Metzner, E. P., Salzmann, M., & Gerdes, R. (2020). Arctic Ocean surface energy flux and the cold halocline in future climate projections. *Journal of Geophysical Research :Oceans*, *125*, e2019JC015554. https://doi.org/10.1029/2019JC015554

Received 8 AUG 2019
Accepted 17 JAN 2020
Accepted article online 29 JAN 2020

The copyright line for this article was changed on 05 MAR 2020 after original online publication.

Abstract Ocean heat transport is often thought to play a secondary role for Arctic surface warming in part because warm water which flows northward is prevented from reaching the surface by a cold and stable halocline layer. However, recent observations in various regions indicate that occasionally, warm water is found directly below the surface mixed layer. Here we investigate Arctic Ocean surface energy fluxes and the cold halocline layer in climate model simulations from the Coupled Model Intercomparison Project Phase 5. An ensemble of 15 models shows decreased sea ice formation and increased ocean energy release during fall, winter, and spring for a high-emission future scenario. Along the main pathways for warm water advection, this increased energy release is not locally balanced by increased Arctic Ocean energy uptake in summer. Because during Arctic winter, the ocean mixed layer is mainly heated from below, we analyze changes of the cold halocline layer in the monthly mean Coupled Model Intercomparison Project Phase 5 data. Fresh water acts to stabilize the upper ocean as expected based on previous studies. We find that in spite of this stabilizing effect, periods in which warm water is found directly or almost directly below the mixed layer and which occur mainly in winter and spring become more frequent in high-emission future scenario simulations, especially along the main pathways for warm water advection. This could reduce sea ice formation and surface albedo.

Plain Language Summary Under the ocean surface, warm water flows from the Atlantic Ocean to the Arctic Ocean. But often it is prevented from reaching the surface by a less salty, and therefore lighter, cold water layer above the warm water. However, recent observations have shown that this cold layer can at times disappear. As long as the warm water from the south stays below this cold and stable layer, warmer ocean currents in a warmer climate might not contribute much to Arctic surface warming. In this study we look at output data from climate models. We find that in a future climate scenario more energy is released from the ocean to the atmosphere, especially in winter. Because in winter the upper meters of the ocean cool down quickly, this energy must come from deeper ocean layers. We find that events in which warm water is not far from the surface occur more often in the future climate simulations than in either past or present-day simulations. This could reduce sea ice formation and surface albedo.

1. Introduction

Arctic surface warming currently proceeds at more than twice the global average rate (Cohen et al., 2014). In principle such an amplification of climate change in the northern polar latitudes is expected based on climate model simulations, paleodata records, and process understanding. Local radiative feedbacks, especially the ice-albedo feedback (active in summer), a lack of atmospheric vertical mixing close to the surface ("Arctic lapse rate feedback"), and the nonlinear temperature dependence of the Stefan–Boltzmann law (Bintanja et al., 2011; Joshi et al., 2003; Pithan & Mauritsen, 2014; Manabe & Wetherald, 1975; Screen & Simmonds, 2010a), are among the factors contributing to Arctic amplification. Arctic climate change is furthermore modulated by atmospheric and oceanic heat transport on various timescales (Laîné et al., 2016; Nummelin et al., 2017; Salzmann, 2017; Spielhagen et al., 2011; Yang et al., 2010) and by increased surface fluxes from the warmer ocean to the atmosphere in the absence of sea ice (Screen & Simmonds, 2010a; Serreze et al., 2009). Ocean processes are sometimes considered of secondary importance, although climate models generally do not agree on the importance of meridional oceanic heat transport in driving Arctic Ocean warming,

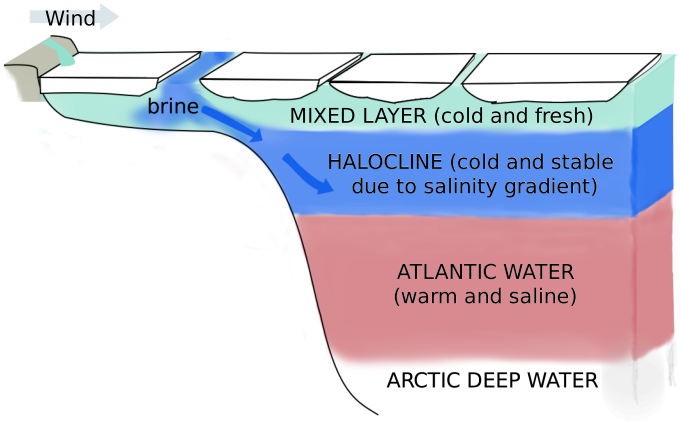

Figure 1. Schematic: Formation of the cold halocline and vertical stratification of the Arctic Ocean. Adapted from Itkin et al. (2015) with permission from the American Geophysical Union.

and many models suggest that meridional oceanic heat fluxes are the main driver of Arctic Ocean warming (Burgard & Notz, 2017). Furthermore, sea ice loss in the Barents sea has previously been linked to heat transport from the Atlantic (Årthun et al., 2012), potentially providing a nonlocal contribution to the surface albedo feedback.

It is, however, not entirely clear how much the Arctic Ocean warming contributes to atmospheric warming. This is because large parts of the Eurasian Basin of the Arctic Ocean are stably stratified. Cold and fresh water in the surface mixed layer is separated from a layer of warm saline Atlantic water by a cold and stable layer, the cold halocline. This cold and stable layer is strongly salt stratified (Carmack, 2007; Carmack et al., 2016), while the underlying Atlantic water is weakly temperature stratified. The halocline layer between the cold surface water and the warm Atlantic water prevents efficient heat exchange between the ocean and the atmosphere and thus to some extent acts similarly to a lid on top of the warmer Atlantic water. The existence of the cold halocline is a prerequisite for sea ice formation. Simulations with a simple column model suggested (Maykut & Untersteiner, 1971) that a small change in upward ocean heat flux would be enough to significantly affect sea ice.

Several mechanisms for the formation of the cold halocline have been suggested. These include salination of cold and fresh surface water, that is, the "convective cold halocline," advection of cold and saline shelf water, which is, however, still less saline than the underlying Atlantic water, and melting of sea ice as Atlantic water enters the ice-covered Arctic shelves (Carmack, 2000; Steele & Boyd, 1998). Fresh water is continuously supplied to the Arctic Ocean primarily by river runoff, import through the Bering Strait, and net precipitation (precipitation minus evaporation) and is lost mainly via export through the Fram Strait and the Davis Strait, either in liquid form or as sea ice (Carmack, 2000; Carmack et al., 2016). A strong salinity gradient in the convective cold halocline is formed mainly in winter during sea ice formation when ice-free regions freeze and brine is released. As seasonal ice zones currently tend to be located in the shelf seas, shelf processes are expected to play an important role in the formation of the halocline. When freezing takes place, cold and saline waters flow away from the shelves and feed into the halocline (Itkin et al., 2015); compare schematic in Figure 1.

Several observation- and model-based studies have suggested an increasing trend in the freshwater supply to the Arctic which is expected to continue in a warming climate due to increasing atmospheric moisture transport from lower latitudes, an intensified hydrological cycle, and increasing river runoff (Bintanja & Selten, 2014; Haine et al., 2015; Peralta-Ferriz & Woodgate, 2015; Zhang et al., 2013). This trend leads to an increased stratification of the upper ocean. On the other hand, observation-based studies (Polyakov et al., 2017; Steele & Boyd, 1998) have indicated that this stable stratification could become weaker in some places as warmer Atlantic water is advected to the Arctic Ocean. Furthermore, heating of the shelf-regions was also found to affect the cold halocline. In particular, Timmermans et al. (2018) attributed increases of ocean heat content in the Beaufort Gyre over the last decades to anomalous solar heating of surface water in the Chukchi

sea, which is a main source for halocline waters entering into the Beaufort Gyre. These observations suggest that advection of warm water and shelf processes are both likely to be important for the cold halocline.

A retreat of the cold halocline was first noted by Steele and Boyd (1998). More recent observations (Polyakov et al., 2017; Timmermans et al., 2018) also suggested that the cold halocline might become even less persistent in a future climate. Therefore, the importance of heat transfer from the ocean to the atmosphere (Polyakov et al., 2010; Screen & Simmonds, 2010b) may increase in the future, especially because the existence of a cold halocline is crucial for sea ice formation (Maykut & Untersteiner, 1971) and because sea ice modulates surface heat fluxes.

Although it is notoriously difficult to establish cause-and-effect relationships in a coupled system, a further retreat of the cold halocline could not only change the partitioning of the total poleward heat transport into the contributions from the ocean and the atmosphere but possibly also contribute to Arctic warming at the surface, which here includes but is not limited to the bottom of the sea ice. Usually, by "surface," we refer to the Earth's surface, that is, the lower boundary of the atmosphere.

While observations are key to understanding climate change, and it is very plausible that anthropogenic greenhouse gas emissions play a role in explaining observed changes, it still remains difficult to link individual observations to climate change without either a long record or climate modeling. The present study demonstrates that results from state-of-the art global climate models generally support the observation-based idea that periods in which temperature stratification plays a large role will increase in the future, in spite of some well-known biases in both the ocean and the atmosphere components of these models. This finding demands further research on the role of the ocean using CMIP-type climate models. To our knowledge, this is the first time that the changes of the cold halocline are studied in the context of global climate models.

In the following section, we introduce the methods used to analyze the Coupled Model Intercomparison Project Phase 5 (CMIP5) model output. We use two different algorithms to define the bottom of the cold halocline, which are based on different characteristics of the cold halocline layer, in an attempt to avoid that key results depend on methodological artifacts. In section 3.1, we investigate changes of surface energy fluxes. In sections 3.2–3.4 we investigate changes in the frequency of cold halocline thinning events in which warm water is found directly below the surface mixed layer. A detailed analysis of the seasonal and spatial distribution suggests that the changes in cold halocline thinning events and the surface energy flux are linked. Correlations between increases in cold halocline thinning event frequency, the decrease of sea ice cover, and the temperature of Atlantic water in the inflow through the Fram Strait and the Barents Sea are investigated in section 3.5.

2. Materials and Methods

2.1. Model Data

Our analysis is based on monthly mean climate model output from the Coupled Model Intercomparison Project Phase 5 (Taylor et al., 2012). In addition to runs from the so-called historical experiment, we analyze output based on the the RCP8.5 high-emission scenario. We start out by analyzing net upward surface energy fluxes. The net energy flux from the ocean including sea ice to the atmosphere is computed as

$$F_s = \mathrm{SHF}+\mathrm{LHF}+\mathrm{F}^{\mathrm{up}}_{s,\mathrm{sw}} + F^{\mathrm{up}}_{s,\mathrm{lw}} - F^{\mathrm{down}}_{s,\mathrm{sw}} - F^{\mathrm{down}}_{s,\mathrm{lw}}, \quad (1)$$

where SHF and LHF are sensible and latent surface heat fluxes, respectively. $F_{s,\mathrm{sw}}$ and $F_{s,\mathrm{lw}}$ are shortwave and longwave surface radiation fluxes.

In addition, we compute diagnostics for the depth of the surface and the cold halocline layers. For this analysis, higher temporal resolution would clearly be desirable. But daily model output of the variables required in this analysis is not available in the CMIP5 data archive. We nevertheless think that using monthly mean data can provide important insights into changes of the cold halocline layer in climate models that contribute to assessment reports such as the Fifth Assessment Report by the Intergovernmental Panel on Climate Change.

Table 1
Models

Model	Center	Reference
CanESM2	Canadian Centre for Climate Modeling and Analysis	Arora et al. (2011)
CCSM4	National Center for Atmospheric Research	Gent et al. (2011)
CNRM-CM5	CNRM and CERFACS[a]	Voldoire et al. (2013)
CSIRO-Mk3-6-0	CSIRO Marine and Atmospheric Researchb[b]	Rotstayn et al. (2012)
GFDL-CM3	NOAA Geophysical Fluid Dynamics Laboratoryc[c]	Donner et al. (2011)
GFDL-ESM2G	NOAA Geophysical Fluid Dynamics Laboratory	Dunne et al. (2012)
GFDL-ESM2 M	NOAA Geophysical Fluid Dynamics Laboratory	Dunne et al. (2012)
GISS-E2-H	NASA Goddard Institute for Space Studiesd[d]	Schmidt et al. (2014)
GISS-E2-R	NASA Goddard Institute for Space Studies	Schmidt et al. (2014)
HadGEM2-ES	Met Office Hadley Centre	Martin et al. (2011)
IPSL-CM5A-LR	Institut Pierre Simon Laplace	Dufresne et al. (2013)
MIROC-ESM	JAMSTEC, AORI, and NIESe[e]	Watanabe et al. (2011)
MPI-ESM-LR	Max Planck Institute for Meteorology	Giorgetta et al. (2013)
MRI-CGCM3	Meteorological Research Institute, Tsukuba, Japan	Yukimoto et al. (2012)
NorESM1-M	Norwegian Climate Centre	Bentsen et al. (2013)

[a]CNRM: Centre National de Recherches Météorologiques, CERFACS: Centre Européen de Recherches et de Formation Avanceé en Calcul Scientifique. [b]CSIRO: Australian Commonwealth Scientific and Industrial Research Organization, in collaboration with the Queensland Climate Change Centre of Excellence. [c]NOAA: National Oceanic and Atmospheric Administration. [d]NASA: National Aeronautics and Space Administration. [e]JAMSTEC: Japan Agency for Marine-Earth Science and Technology, AORI: Atmosphere and Ocean Research Institute, The University of Tokyo, NIES: National Institute for Environmental Studies, Ibaraki, Japan.

The historical experiment spans the years 1850 to 2005. In this experiment, estimates of historical greenhouse gas concentrations and aerosol emissions are combined with estimates of volcanic and solar forcings in an attempt to arrive at simulations of Earth's climate from 1850 to 2005 that are, within the range of internal variability, compatible with observations. Although, for most of the models, several historical runs with slightly perturbed initial conditions were performed within the framework of CMIP5, here we analyze only one run, that is, the first realization in the standard configuration, per model. In order to find out how a failure to reduce greenhouse gas emissions may affect the cold halocline layer, we also analyze the CMIP5 RCP8.5 "high-emission" future scenario.

For evaluating the vertical structure in the Arctic upper ocean, potential temperature, salinity, and sea ice cover data are analyzed. The bottom of the cold halocline and the mixed layer, the cold halocline thickness, and the frequency of cold halocline thinning events are computed based on potential temperature and salinity as described below. Data were obtained for the models listed in Table 1. The ocean components of 11 of the 15 coupled models feature at least 9 or 10 vertical layers in the upper 100 m, many of them at a uniform spacing of 10 m and between 15 and 21 layers in the upper 200 m. The two GISS models and the CSIRO model in this study use only between 6 and 11 layers in the upper 200 m. The vertical grid spacing in the upper 50 m is 10 m in all models except for the following: In GISS-E2-H it ranges from 10 to 20 m, in GISS-E2-R from 15 to 31 m, in MIROC-ESM from 5 to 9 m, in MRI-CGCM3 from 2 to 13 m, in MPI-ESM-LR from 11 to 10 m, and in NorESM from 5 to 10 m.

2.2. Diagnostics

The lower boundary of the cold halocline is computed using two different algorithms. The first algorithm follows Bourgain and Gascard (2011). We refer to this algorithm as the density ratio algorithm. The density ratio is given by

$$R_\rho = \left[\alpha \frac{\mathrm{d}\theta}{\mathrm{d}z}\right] / \left[\beta \frac{\mathrm{d}S}{\mathrm{d}z}\right], \tag{2}$$

where θ is potential temperature in K, S is salinity in PSU, ρ potential density in kg m^{-3}, z depth in m, $\alpha = \rho^{-1}(\partial\rho/\partial\theta)$, and $\beta = \rho^{-1}(\partial\rho/\partial S)$ are the thermal expansion coefficient and the haline contraction

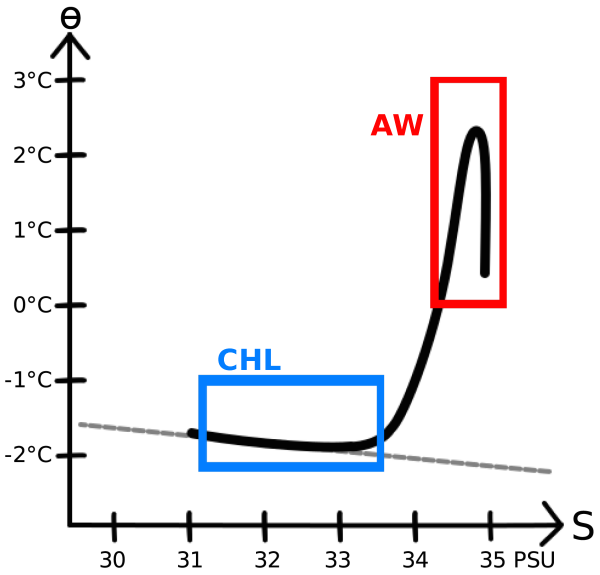

Figure 2. Schematic: potential temperature-salinity diagram. Potential temperature θ and salinity S in the Arctic Ocean with distinct cold halocline layer (CHL, blue) and Atlantic water (AW, red). The gray line indicates the freezing temperature as a function of salinity.

coefficient, respectively. The density ratio represents the slope in the temperature(θ)-salinity(S) diagram scaled by α and β (Figure 2). The bottom of the cold halocline is defined as the depth of the first layer from the top down where R_ρ exceeds 0.05. This threshold was determined empirically from observations (Bourgain & Gascard, 2011). It provides a measure of the transition from a halocline to a thermocline.

In the second algorithm, the lower bound of the cold halocline is determined by a temperature difference of 1 K between water potential temperature and its freezing temperature T_{freeze}. We call this the temperature difference algorithm. The definition is motivated by the notion that freezing plays an important role in the formation of the cold halocline layer (compare schematic in Figure 1). A second condition is that the potential temperature should increase with depth. This avoids misinterpretations in case of warm water at the surface. Based on Figure 5 of Carmack et al. (2016), the 1 K difference appears to be a good choice for the Eurasian Basin, while for the Amerasian Basin 1.5 K might be a better choice. The thinning event frequencies (defined below) are, however, not very sensitive to this choice. The freezing temperature in °C is computed from (Gill, 1982):

$$T_{\text{freeze}} = -0.0575\ S + 1.710523\cdot 10^{-3}\ S^{1.5} - 2.154996\cdot 10^{-4}\ S^{2} - 7.53\cdot 10^{-3}\ p, \quad (3)$$

where pressure p in bar is calculated iteratively from the temperature and salinity profiles as follows: At first, density is computed based on equations A3.1 to A3.6 from Gill (1982) using a first guess for pressure. Then, the hydrostatic equation is solved using the resulting density profile. These computations are repeated until the resulting error becomes negligible.

Each algorithm focuses on different characteristics of the cold halocline layer. The density ratio algorithm indirectly takes into account the stability formed by temperature, salinity, and density gradient. But it is calculated only over few data points (vertical model layers) in each water column, and the salinity gradient is in the denominator (equation (2)), which makes it very sensitive to the salinity profile.

The temperature difference algorithm is highly sensitive to warming from below, which is of interest in the present study. It produces fewer missing values when the condition for identifying the cold halocline layer bottom is not met in the first 400 m below the surface mixed layer. The 400 m requirement avoids misidentifying the bottom of the cold halocline below the core of the warm Atlantic water.

In addition to the bottom of the cold halocline, we also diagnose the bottom of the surface mixed layer. Here, it is defined by an increase of potential density of 0.125 kg m^{-3} from the ocean surface as in, for example, Polyakov et al. (2017).

The cold halocline layer thickness is determined as the difference between the bottom of the cold halocline layer and the bottom of the surface mixed layer. When the cold halocline layer thickness based on monthly average model output decreases below 10 m, we define this as a "thinning event." The probability of a cold halocline thinning event is computed by dividing the number of months in which the monthly mean layer thickness is below 10 m by the total number of months in the period for which the probability for the occurrence of a thinning event is computed.

The direction of a multimodel mean change is deemed to be significant at the 95% level based on a threshold for the number of models in which the sign of the change agrees with the sign of the change of the multimodel mean allowing for missing values. In order to obtain a 95% significance level, at least five models have to provide nonmissing values. In the case of only five nonmissing values, all five models have to agree on the sign of the change. Where nonmissing values for all 15 models are available, the minimum number of models that have to agree on the sign in order to obtain a 95% significance level increases to 12 out of 15 based on a binomial distribution. The Community Climate System Model Version 4 is left out for the density ratio algorithm due to a problem in determining the cold halocline layer in the historical run.

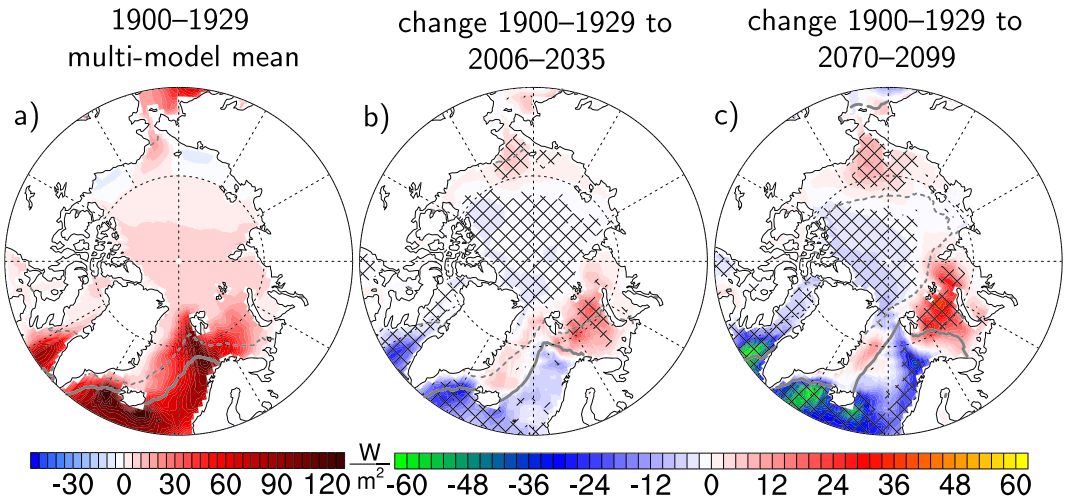

Figure 3. Multimodel mean upward surface net energy flux over ocean and sea ice (sum of radiative, sensible heat, and latent heat fluxes) and projected changes for the models listed in Table 1 for the CMIP5 RCP8.5 high-emission scenario. (a) 1900–1929 multimodel mean, (b) change from 1900–1929 to 2006–2035, (c) change from 1900–1929 to 2070-2099. Hatching in (b) and (c) indicates areas where the direction of the multimodel mean change is significant at the 95% level. The average sea ice edge for spring (MAM) and for fall (SON) is indicated by a solid and a dashed gray line, respectively.

3. Results

3.1. Surface Energy Fluxes

Figure 3a shows multimodel annual mean net upward surface energy fluxes for the models listed in Table 1 for the years 1900 to 1929. Positive upward net surface energy fluxes indicate that ocean heat transport warms the atmosphere. Large positive fluxes are mainly found along the main pathways of warm water inflow from lower latitudes, especially in the Barents Sea and the Chukchi Sea. Note that both the ocean and the atmosphere transport heat from lower latitudes to the Arctic.

Changes of the multimodel annual mean net surface energy fluxes relative to 1900 to 1929 for the years from 2006 to 2035 and for the years from 2070 to 2099 are shown in Figures 3b and 3c, respectively. The spatial patterns of the changes in Figures 3b and 3c are similar. The multimodel annual mean net energy fluxes from the ocean to the atmosphere increase along the main pathways of warm water inflow in the Barents Sea, the Kara Sea, and the Chukchi Sea, while on average, the models show only small changes in the Laptev Sea. However, individual models such as CanESM2 and HadGEM2-ES show increased annual mean upward energy fluxes in the Laptev Sea as well (Figure S1 in the supporting information), and for individual seasons (Figure 4), the multimodel average does show changes in the Laptev Sea. However, these seasonal changes can be balanced locally. In particular, an increased energy release from the ocean to the atmosphere in winter can be balanced by additional energy uptake in summer. The annual mean changes in Figures 3b and 3c, on the other hand, are not balanced locally.

Inspecting the seasonal means in Figure 4 shows that the multimodel mean energy release from the ocean to the atmosphere increases during winter. In the absence of other heat sources, this additional energy can only be supplied to the upper ocean mixed layer by increased heat supply from the underlying warm water. In summer, on the other hand, the ocean serves as an energy sink for the atmosphere. The imbalance in the changes of the annual mean surface energy fluxes in Figure 3b together with the seasonality of the changes suggests that ocean heat transport plays a role. Furthermore, the area of positive changes in the annual mean net energy fluxes in Figures 3b and 3c expands over time. Annual mean changes in the Amerasian Basin are smaller in magnitude and of opposite sign. This indicates that atmospheric warming dominates the change in surface energy fluxes in the Amerasian Basin. An increased annual mean net positive energy flux from the ocean to the atmosphere is found in the Barents and the Kara Sea, in the Chukchi sea, and in some models also south of the Fram Strait.

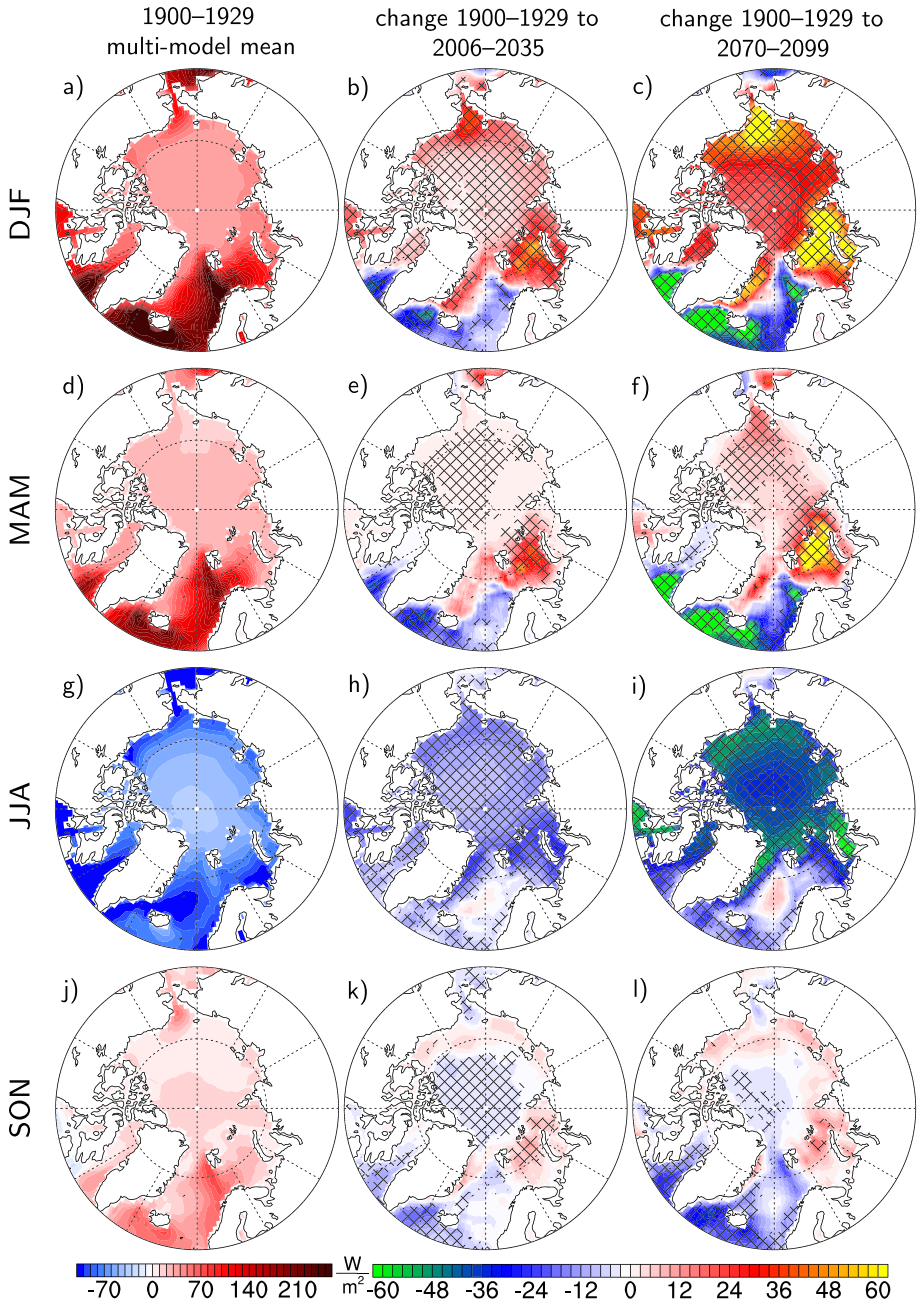

Figure 4. Seasonal mean upward surface net energy flux (as in Figure 3) for (a–c) DJF, (d–f) MAM, (g–i) JJA, and (j–l) SON.

3.2. Cold Halocline Diagnostics

Figure 5 shows time series of upper ocean temperature, salinity, and the logarithm of the squared Brunt-Väisälä-Frequency N (N in s^{-1}) at a selected grid point in the vicinity of 125.7°E 81.1°N (point M1 in Figure S2) from the CanESM2 model. The corresponding plots for other models are shown in Figures S3 and S4. While a few models simulate an overly smooth temperature gradient in the upper 200 m compared to observations (Polyakov et al., 2017) in this region, CanESM2 does well in this aspect.

Figure 5a shows increasingly warmer water below the cold halocline layer. Zooming in on the end of the century in Figure 6 shows that in summer, the mixed layer deepens to the depth of the warm water below, as indicated by negative slopes in the temperature contours in spring down to about 50 m depth. Below 50 m, positive slopes indicate that over the annual cycle warm water, which does not seem to originate in the

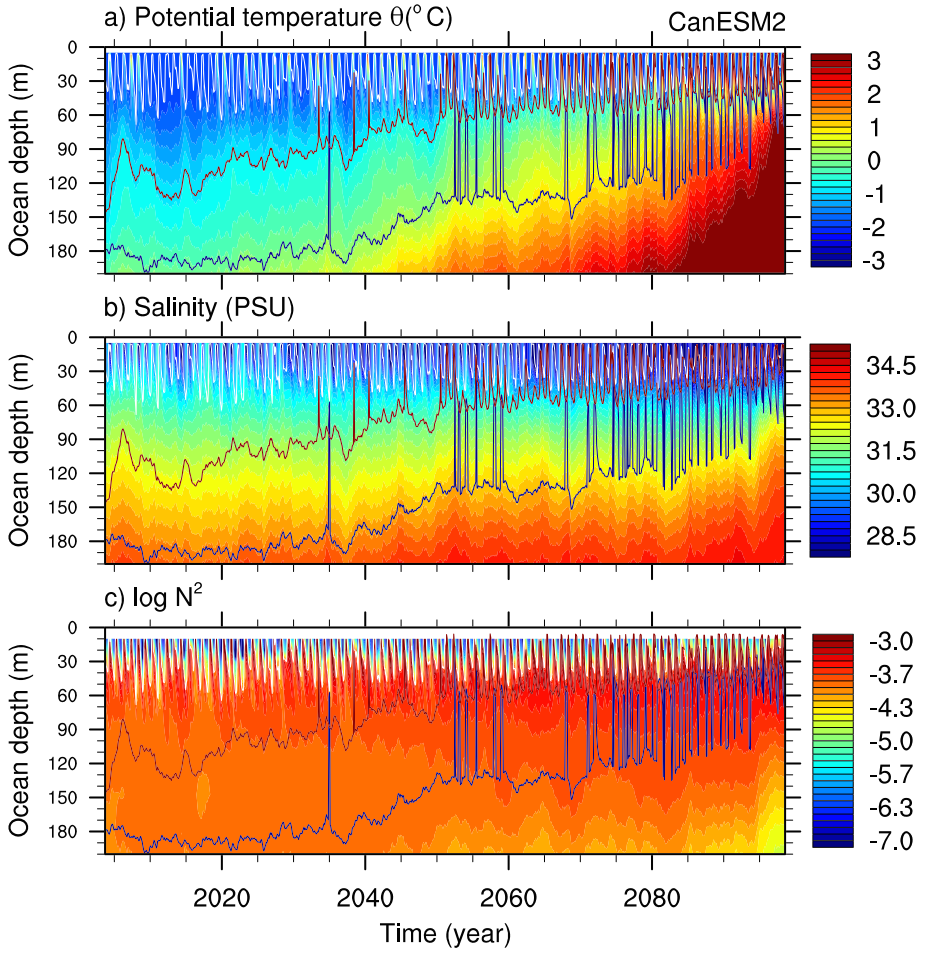

Figure 5. Monthly mean upper ocean (a) potential temperature, (b) salinity, and (c) logarithm of the squared Brunt-Väisälä-Frequency N (N in s^{-1}) at 125.7°E 81.1°N (point M1 in Figure S2) for the RCP8.5 "high-emission" scenario from the Canadian CanESM2 coupled climate model from 2006 to 2100. The white line is the bottom of the surface mixed layer (here defined by a density increase of 0.125 kg m^{-3} from the surface as in Polyakov et al., 2017). The two dark lines show the bottom of the cold halocline layer computed from monthly mean data with the temperature difference algorithm (red, this is the upper dark line) and from the density ratio algorithm (blue, this is the lower dark line). Corresponding plots for other models are shown in Figures S3 and S4.

mixed layer directly above in the same column, comes closer to the mixed layer. In summer, this could be a signature of warming in the shelf seas as suggested by Timmermans et al. (2018). Warm water in winter most likely originated at lower latitudes as previously suggested by Polyakov et al. (2017) (see also section 3.3).

The largest temperature gradients below the bottom of the mixed layer are found in winter and spring, when at times the diagnosed bottom of the cold halocline reaches close to the bottom of the mixed layer. Consequently, most halocline thinning events are diagnosed in winter and spring (compare section 3.4). Although the density ratio algorithm usually diagnoses the cold halocline to extend further downward than the temperature difference algorithm, halocline thinning events are diagnosed by both algorithms, and both algorithms show an increase in the frequency of these events over time. Because the density ratio algorithm is sensitive not only to the temperature but also to salinity, it places the bottom of the cold halocline in CanESM2 below the cold homogeneous layer. This also applies to several other models (Figures S3 and S4). In a few models, however, both algorithms place the bottom of the cold halocline at similar depth. We are currently evaluating these differences based on observations.

While the Atlantic warm water extends upward, the mixed layer, which is thickest in winter, becomes shallower over time. This thinning could be caused either by decreased surface cooling or by mixing of warm

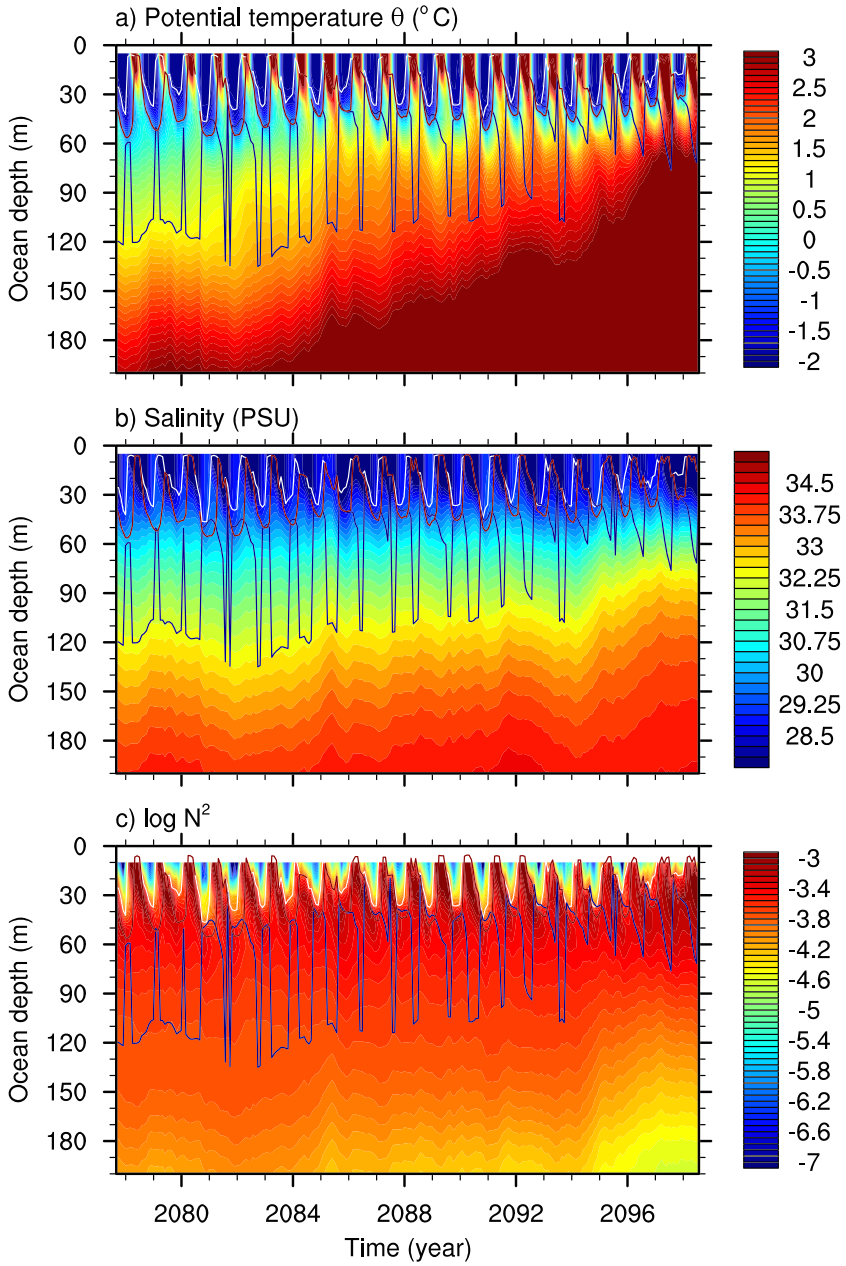

Figure 6. (a–c) Figure 5 zoomed in on upper ocean in the end of the 21st century.

water from below. The finding that surface energy fluxes from the ocean to the atmosphere increase in winter indicates that not only decreased surface cooling but also mixing of warm water from below is likely to play a role for sea ice formation and the surface albedo feedback.

Figure 5b also shows a signature of increased freshwater input from 2006 to 2100 as expected based on existing literature (Bintanja & Selten, 2014; Haine et al., 2015). Increased freshwater input leads to a larger salinity gradient below the surface mixed layer and thus a stabilization toward the end of the century (Figure 5c). An increased salinity gradient due to the input of freshwater is found not only in the CanESM2 model but also in several other models (Figures S3 and S4). However, at the same time, cold halocline thinning events during which warm water is located directly below the cold surface mixed layer in winter and spring become more frequent. Thus, overall, the stabilization due to the increased salinity gradient does not prevent an increase in the frequency of halocline thinning events. Instead, large temperature gradients below the surface mixed layer, which have a destabilizing effect, are found in winter. Figure 5c shows both, destabilization

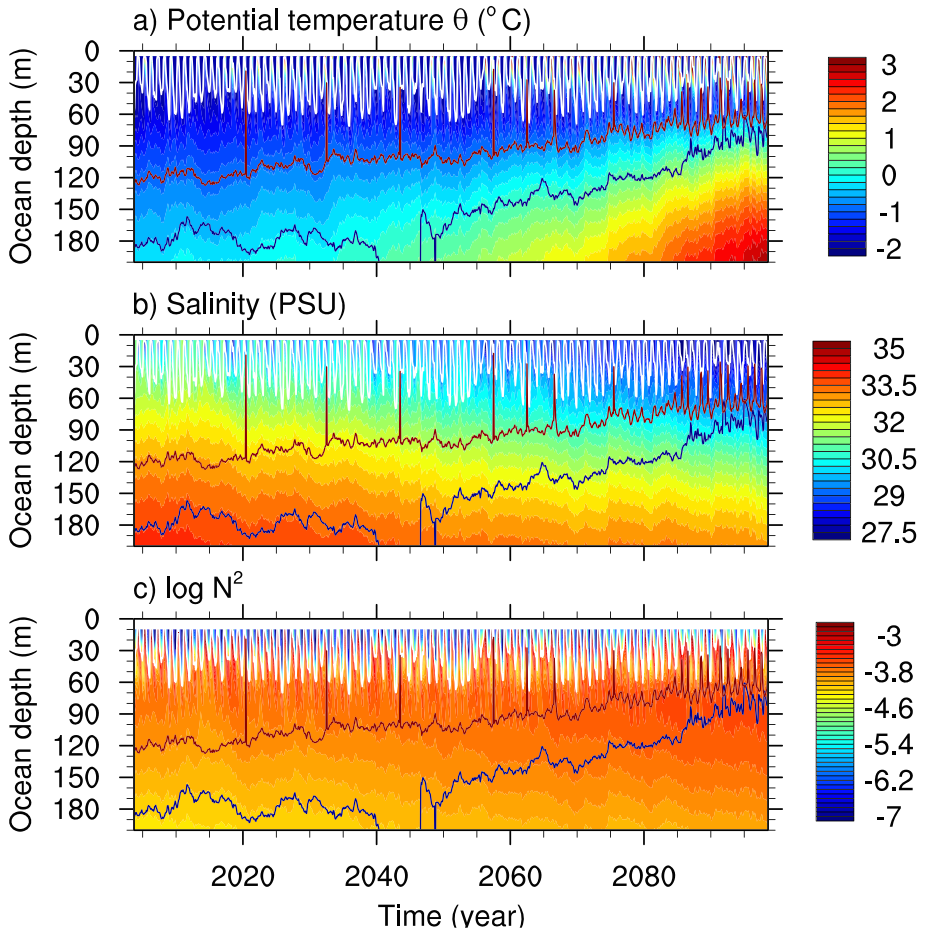

Figure 7. As in Figure 5 but for 145.0°W 74.0°N (point A1 in Figure S2).

from below due to an increasing temperature gradient and the stabilizing effect of fresh water. Toward the end of the century, in summer, warm water in the surface mixed layer is no longer clearly separated from the warm water below.

A back-of-envelope computation for this CanESM2 vertical column shows that the thickness of sea ice that could be melted by Atlantic warm water between the bottom of the cold halocline layer and 300 m depth increases from less than 5 m in the beginning of the 21st century to more than 20 m in the end of the 21st century. Multimodel mean increases in potential temperature at 300 and at 400 m depth are shown in Figures S5 and S6, respectively.

Saline water enters the Arctic primarily from the Atlantic. Pacific water entering the Arctic is less saline, and the Bering Strait is comparatively shallow. Consequently, one would expect differences between the Eurasian and the Amerasian Basin also in the CMIP5 model runs. A fundamental difference between the projected salinities is illustrated by comparing Figures 5b and 6b to Figures 7b and 8b for a grid point in the Amerasian Basin. The former two figures show an increasing salinity gradient which is consistent with increasing atlantification (Årthun et al., 2012; Polyakov et al., 2017) and freshening near the surface. As mentioned above, this increasing salinity gradient has a stabilizing effect, while the increasing temperature gradient has a destabilizing effect. The latter two figures also show freshening down to about 90 m at the end of the century. But unlike the corresponding figures for the grid point in the Eurasian basin, the figures for the grid point in the Amerasian Basin show decreasing salinity below 90 m. A similar tendency is found in several other models (Figures S7 and S8). The temperature gradient, however, increases in the Eurasian and the Amerasian Basins (Figures 7a and 8a). While halocline thinning events at the grid point in the Eurasian Basin are related to warm water underlying cold water throughout winter and spring (Figure 6a),

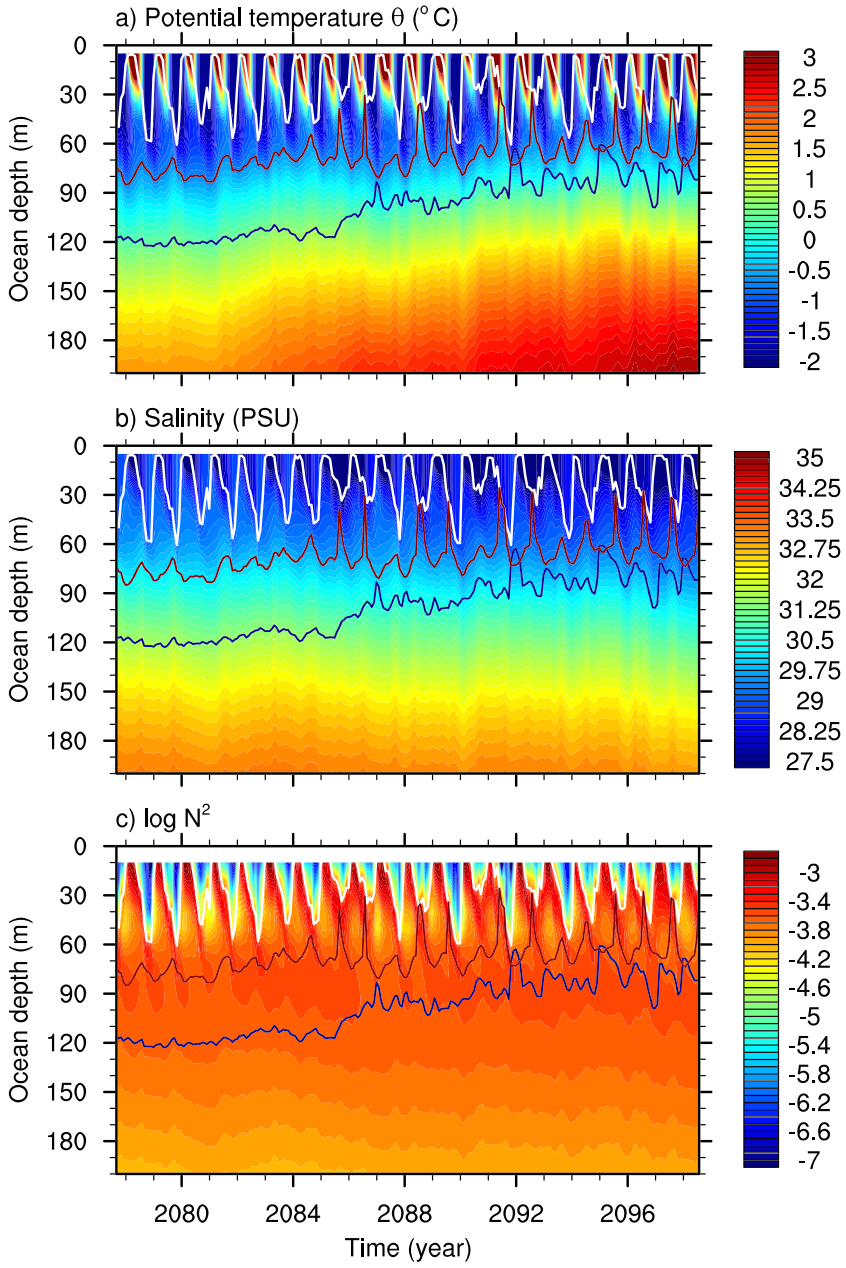

Figure 8. As in Figure 6 but for 145.0°W 74.0°N (point A1 in Figure S2).

the thinning events at the grid point in the Amerasian Basin occur mainly in the beginning of the cold season. This might be explained by a lack of warm water supply below.

In order to better understand the origin of the differences between Figures 5 and 7, we analyze the potential temperature and salinity profiles down to 400 m along a transect in Figures 9 and 10. The transect starts at a selected grid point in the Bering Strait, crosses the North Pole, and ends in the Norwegian Sea. Corresponding plots for a transect that passes through point A1 but starts at the Canadian coast instead of the Bering Strait are shown in Figures S9 and S10. Warm and saline water is advected from the Atlantic into the Arctic, where mixing and cooling from above take place. Previous studies have shown that Atlantic water is advected along the Eurasian continental slope and spreads throughout the Arctic Basin at depths between roughly 200 and 800 m (Carmack et al., 2015; Newton & Coachman, 1974; Rudels et al., 1994). The vertical salinity and temperature gradients below the surface mixed layer in the the Eurasian as well as the Amerasian Basin in Figures 9 and 10 reflect the signatures of advection, freshening and cooling from above,

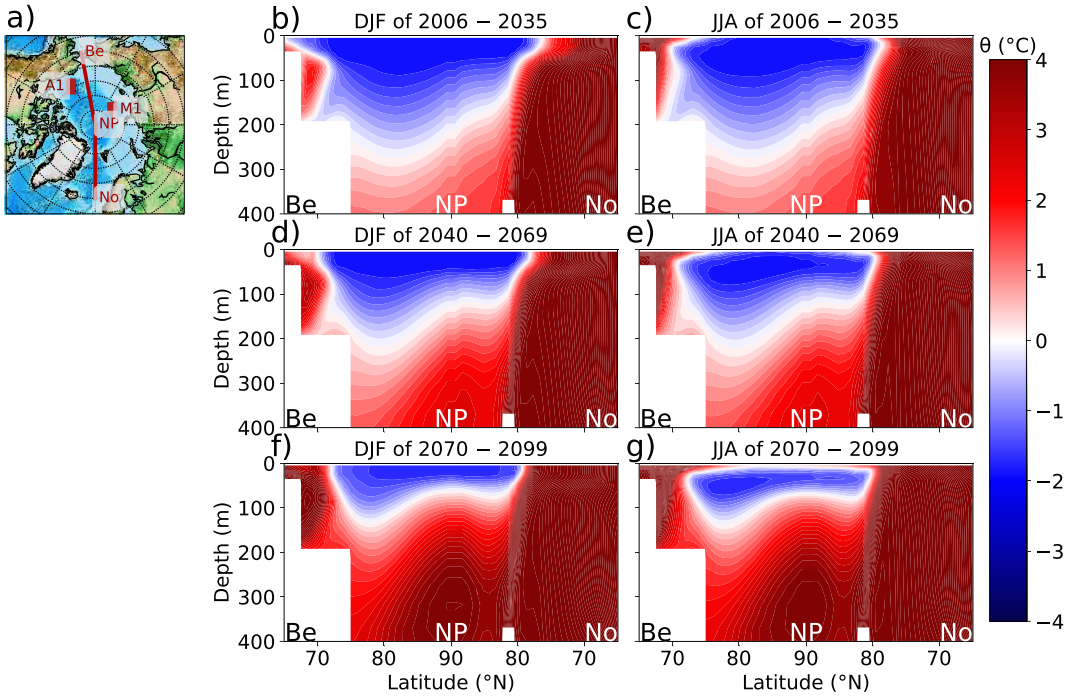

Figure 9. (a) Map showing the location of points M1, A1, and a transect starting at a selected grid point in the Bering Strait (Be), crossing the North Pole (NP), and ending in the Norwegian Sea (No). (b–f) Potential temperature θ in the upper 400 m from CanESM for the RCP8.5 scenario for the Be-NP-No transect.

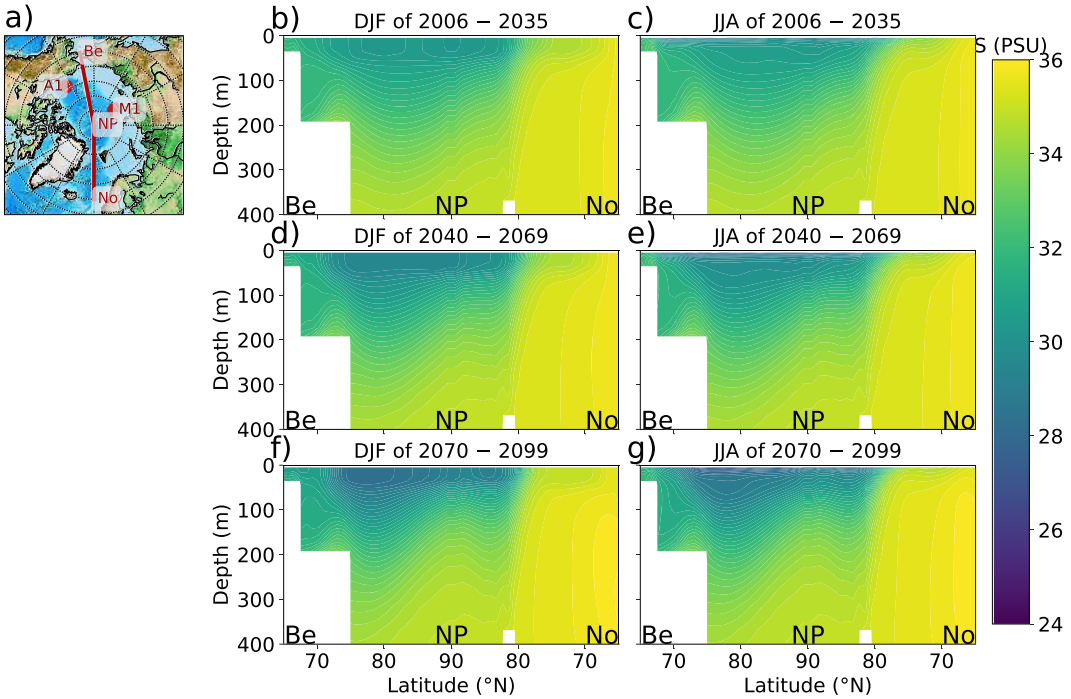

Figure 10. As in Figure 9 but for salinity (S).

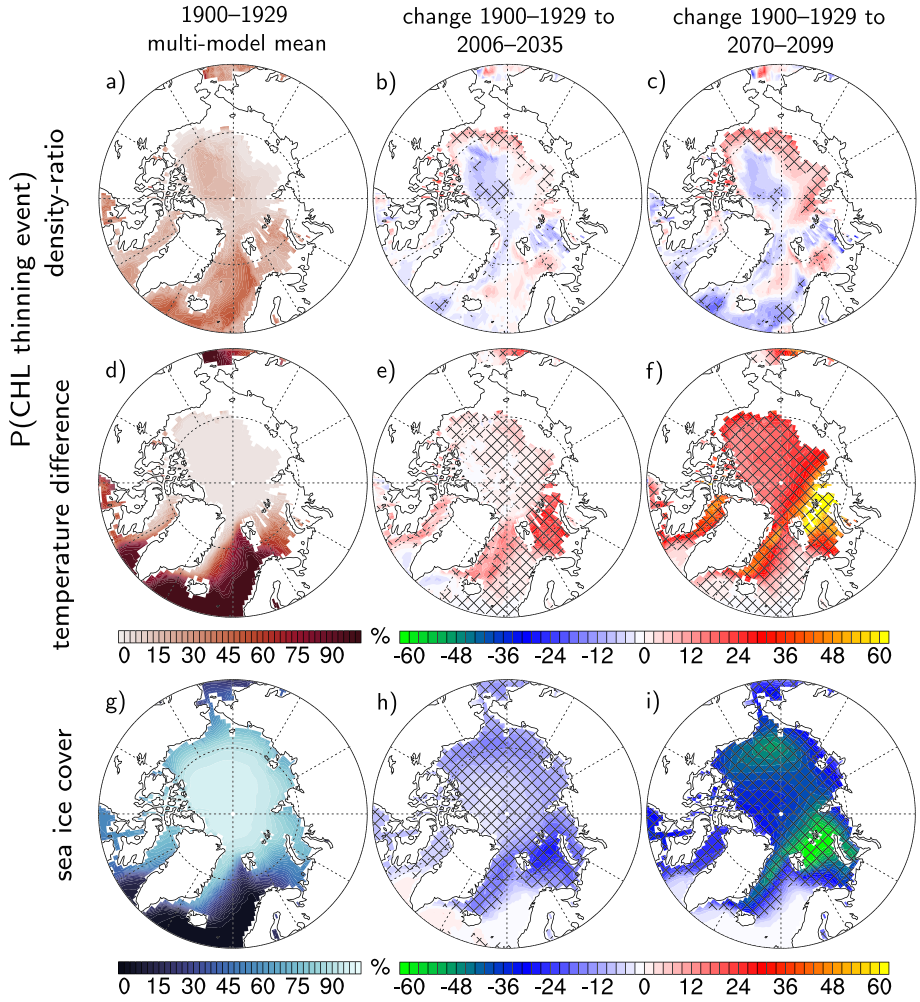

Figure 11. (a) CMIP5 multimodel mean halocline thinning event probability in percent for regions with a minimum water depth of 100 m based on monthly mean data for the months from 1900 to 1929 computed with the density ratio algorithm. (b, c) Change in thinning event probability for the CMIP5 RCP8.5 "high-emission" scenario for 2006 to 2035 and 2070 to 2099 relative to 1900 to 1929 based on the density ratio algorithm. The change is defined in terms of the total thinning event probability. For example, 20% change in a region with a 20% probability corresponds to a doubling of the thinning event probability. (d–f) Same as (a–c) but for the temperature difference algorithm. (g) Multimodel mean sea ice cover in percent for 1900 to 1929 and (h, i) change. Hatching indicates areas where the direction of the multimodel mean change is significant at the 95% level. This is a measure of how many signs of the changes from the individual models agree (see section 2 for details). The annual cycle of the changes in thinning event frequency is shown in Figure 12. The annual cycle of the thinning event frequency for the region around M1 in Figure S2 is shown in Figure 13.

and the influence of vertical and horizontal mixing. Warm and saline water, owing its characteristics in part to inflow from the Atlantic, is found at greater depth in the Amerasian Basin than in the Eurasian Basin. While this geographical difference persists throughout the century, the depth of the warm and saline water decreases in both basins. Toward the end of the century, warm water stretches from the Atlantic to the Bering Strait. The salinity in the warm and saline water in the basins is, however, still higher than the salinity in the Bering Strait, in spite of the freshening in Figure 7b. This suggests that Atlantic warming not only affects the Eurasian Basin but also the Amerasian Basin. While the term atlantification suggests an increasingly saline upper ocean, freshening above the warm and saline water takes place across much of the basin. The resulting stabilization is counteracted by an increasing temperature gradient, which also leads to an increase of the density ratio. Warm water below the mixed layer as in Figures 6a and 8a suggests that stabilization due to freshening is insufficient to prevent halocline thinning events and to shut off heat release from the ocean to the atmosphere.

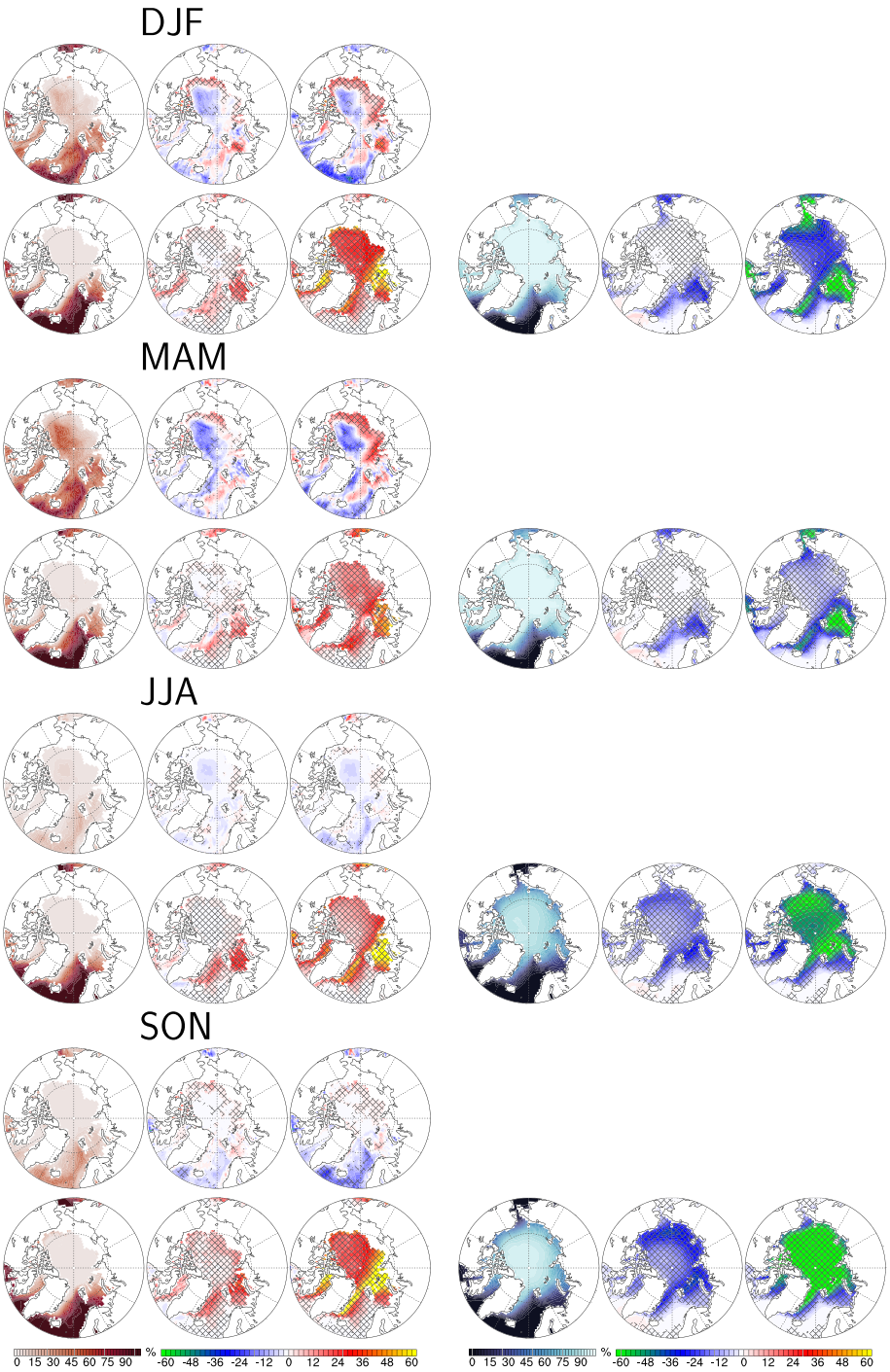

Figure 12. As in Figure 11 but for different seasons. Left column: thinning event probabilities. Left column, upper rows: based on density ratio algorithm. Left column, lower rows: based on temperature difference algorithm. Right column: sea ice.

3.3. Spatial Distribution of Halocline Thinning Events

Figures 11a–11f shows multimodel mean maps of cold halocline layer thinning event probabilities based on monthly mean climate model output for CMIP5 historical model simulations and simulations of the CMIP5 RCP8.5 high-emission future scenario. In spite of considerable spread between models (see Figures S11 and S12 for results from individual models) and less frequent thinning events diagnosed with the density ratio algorithm, which unlike the temperature difference algorithm takes into account salinity, overall the models

tend to simulate more frequent cold halocline layer thinning events in the future for the RCP8.5 scenario (Figures 11a–11f). This suggests that without greenhouse gas emission reductions, the cold halocline would become more prone to thinning events in the future. Large changes of the halocline thinning event frequency toward the end of this century are found outside the coastal regions in the shelf seas, along the slopes, and in the Beaufort Sea. Statistically significant changes are also found in the northern part of the Eurasian Basin. For the density ratio algorithm, a decrease of the frequency of halocline thinning events is found in parts of the Barents sea. However, inspecting temperature and salinity plots from a location in this region suggests that this is an artifact (not shown). Near the coast, in the shallow parts of the shelf seas, a well-defined cold halocline does not exist. Therefore, Figures 11a–11f show shaded contours only for regions in which the water depth exceeds 100 m.

As a possible mechanism for the increase in thinning event frequency, northward warm water advection and subsequent destabilization from below has been suggested (Polyakov et al., 2017). Indeed, the increase in thinning event frequency and the sea ice cover retreat in Figures 11g–11i broadly follow the influx of Atlantic warm water into the Eurasian Basin via the Fram Strait and the Barents Sea (Aksenov et al., 2010). In the Amerasian Basin, a pronounced increase in the frequency of halocline thinning events and sea ice loss is simulated in the Beaufort Gyre region. A recent study (Timmermans et al., 2018) attributed increases of ocean heat content in the Beaufort Gyre over the last decades to anomalous solar heating of surface water in the Chukchi sea which is a main source for halocline waters entering into the Beaufort Gyre. Woodgate (2018) also found increasing inflow of Pacific water entering through the Bering Strait. The CMIP5 models suggest increases in cold halocline thinning event frequency already in the "near-present" years 2006–2035 for this region (Figure 11b). As discussed above, Figures 9 and 10 suggest that in addition, warmer Atlantic water also affects the Amerasian Basin.

Increased warm water advection also appears to be consistent with Figure 5 which shows results for a selected grid point in the vicinity of 125.7°E 81.1°N (point M1 in Figure S2) for a single climate model. It also appears to be supported by several other models (see Figures S3 and S4), although the spread between the models is large. On the other hand, warm water advection and destabilization from below may not be the only processes that play a role for increased probability of halocline layer thinning events in Figure 5. In particular, as Timmermans et al. (2018) and also the schematic in Figure 1 indicate, it is plausible that warming has slowed the halocline formation. A slowed halocline formation would also explain the relatively low salinity of the warm water below the mixed layer in winter. Therefore, further studies focusing on the role of shelf processes are needed.

3.4. Seasonality of Cold Halocline Thinning Events

Although the two algorithms suggest a slightly different seasonality of the increase in halocline thinning event frequency, the largest increase of cold halocline thinning event frequency is found in winter and spring, the latter especially for the density ratio algorithm (Figure 12). Winter and spring are also the seasons in which halocline thinning events tend to be frequent in most of the models. (The annual cycle of the thinning event frequency for the region around M1 in Figure S2 is shown in Figure 13.) These thinning events could, however, in principle also affect sea ice cover in summer because of the ice-albedo effect. This is because decreased sea ice formation results in younger and thinner summer ice forming cracks earlier and melting faster.

Seasonality is also crucial for relating changes of surface energy fluxes to cold halocline thinning. On the one hand, it is in winter that the warm ocean water acts as the main heat source for the upper ocean mixed layer, while in summer, the ocean surface is also heated. On the other hand, cold halocline thinning events are found to be most frequent in winter and spring. Therefore, it seems more appropriate to compare the changes of surface energy flux in winter (Figures 4b and 4c) and spring (Figures 4e and 4f) to the corresponding panels in Figure 12 rather than to compare annual means. The spatial patterns in Figures 4b, 4c, 4e, and 4f are especially similar to the corresponding patterns for the temperature difference algorithm in Figure 12. The corresponding pattern correlations (Pearson coefficients r) are 0.55, 0.77, 0.45, and 0.65. The similarity between the patterns in Figures 11b and 11c and the patterns in Figures 3b and 3c, on the other hand, could also be a consequence of surface warming in summer.

3.5. Correlation With Sea Ice and Inflow of Atlantic Water

Figures 11g–11i show that at the same time as the cold halocline thinning event frequency is increasing in the model runs, there is also a retreat of the sea ice. Furthermore, Figures 14a and 14b show that models which

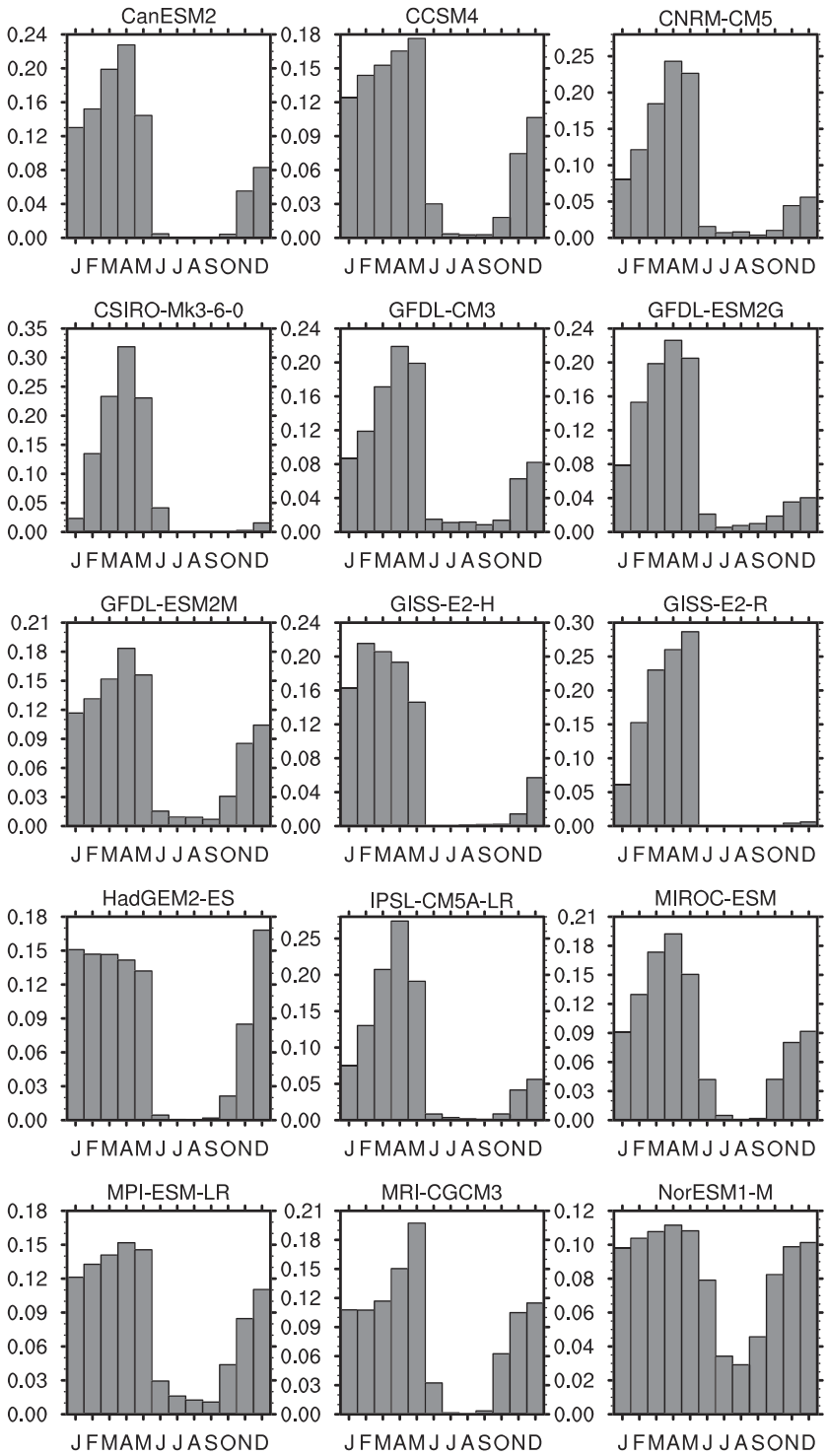

Figure 13. Monthly cold halocline layer thinning event probability for the region around M1 shown in Figure S2 for 2006 to 2035 in the RCP8.5 model runs based on the density gradient algorithm.

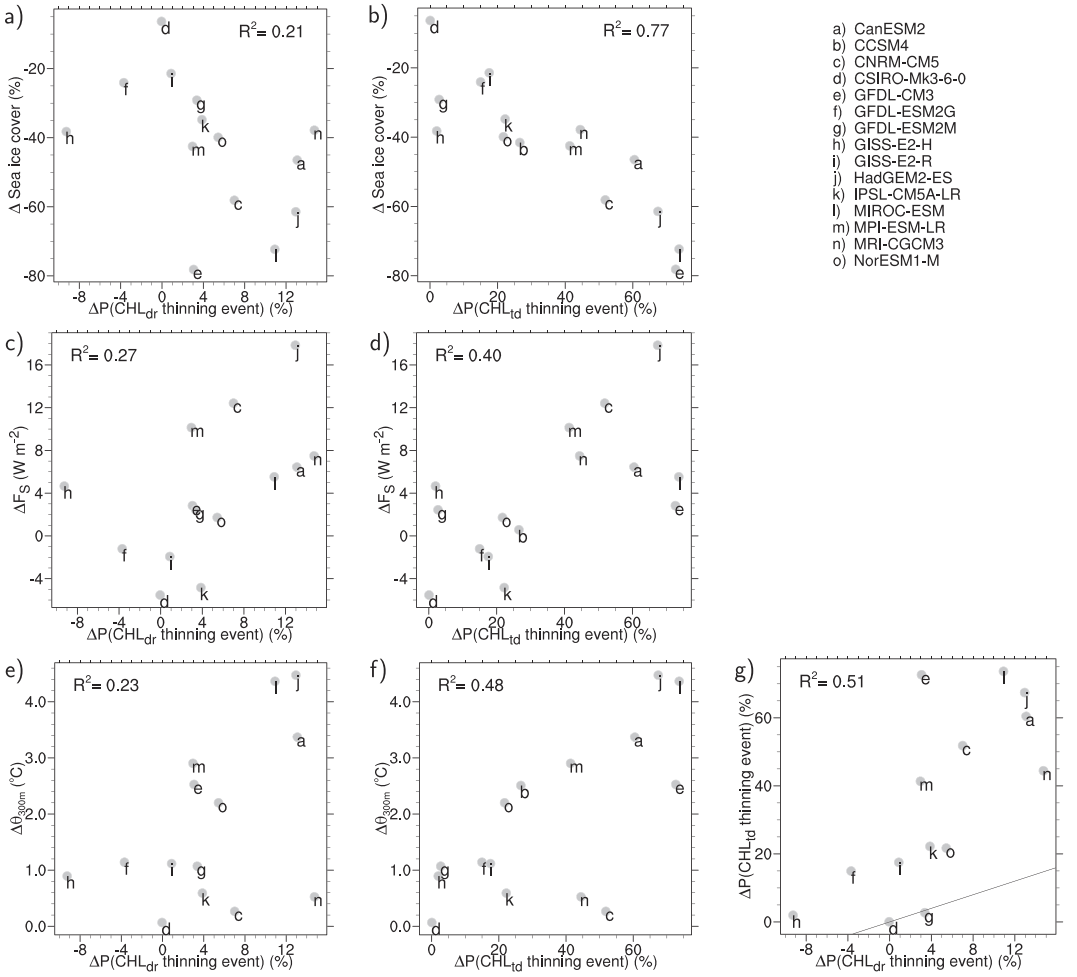

Figure 14. (a, b) Correlation between the change of the cold halocline layer thinning event probability and the change of sea ice cover for the region from 60.0°E to 150.0°E longitude and 75.0°N to 85.0°N latitude (shown in Figure S2) from 1900–1929 to 2070–2099 for the climate models in Table 1. The cold halocline layer depth was computed using (a) the density ratio algorithm (index "dr") and (b) the temperature difference algorithm (index "td"). (c, d) As in (a,b) but for surface heat flux instead of sea ice cover. (e, f) Correlation between the change of the cold halocline layer thinning event probability for the region from 60.0°E to 150.0°E longitude and 75.0°N to 85.0°N latitude with the change of the potential temperature at 300 m depth in the region from 30.0°W to 20.0°E longitude and 65.0°N to 75.0°N latitude (also shown in Figure S2) where Atlantic water enters the Arctic through the Fram Strait and the Barents Sea. (g) Correlation between the cold halocline layer thinning event probability computed with the density ratio and the temperature difference algorithm for the same region also showing the one-to-one line. Data from the CMIP5 historical and the CMIP5 RCP8.5 "high-emission" scenario experiment were used.

simulate a strong increase of the cold halocline layer thinning event probability also tend to simulate a larger sea ice retreat in a warmer climate. The change in surface energy fluxes is also correlated to the change of the probability of cold halocline layer thinning events (Figures 14c and 14d). Furthermore, models in which the Atlantic water potential temperature at 300 m depth increases most strongly in the region from 30.0°W to 20.0°E longitude and 65.0°N to 75.0°N latitude also tend to show a larger increase of the thinning event frequency in the Arctic Ocean region from 60.0°E to 150.0°E longitude and 75.0°N to 85.0°N (Figure S2) as evidenced by the positive correlation in Figures 14e and 14f. The region from 30.0°W to 20.0°E longitude and 65.0°N to 75.0°N latitude is a region where inflow from the Atlantic takes place. In this region, warm water from the Atlantic enters the Arctic through the Fram Strait and the Barents Sea.

Finally, the differences in the changes of cold halocline layer thinning event probabilities that result from using two different algorithms for computing the depth of the halocline are compared in Figure 14g (see also Figure S13 for a comparison of the cold halocline average depth). Although the algorithms focus on different characteristics of the cold halocline layer, they yield qualitatively similar results with respect to the

change of the thinning event frequency. Both algorithms suggest an increase in halocline thinning event frequency in a warmer climate.

While the previous discussion focused on the effects of temperature and salinity, dynamics changes can also influence the cold halocline. In particular, based on CMIP5 simulations, the polar high is expected to weaken in the future (Figure S14a). This weakening is expected to influence the occurrence of seasonal ice (Figure S14b), which is partially wind driven. Sea ice affects the cold halocline in multiple ways (see Figure 1), and there may also be more direct dynamical linkages.

4. Conclusions and Discussion

An ensemble of 15 climate models from the Coupled Model Intercomparison Project Phase 5 (CMIP5) shows that ocean energy release increases during fall, winter, and spring for a high-emission future climate change scenario. This increased energy release is not locally balanced by increased Arctic Ocean energy uptake in summer along the main pathways for warm water advection.

Because increased ocean surface energy release cannot be explained by atmospheric warming in the Arctic, and because during Arctic winter, the ocean mixed layer is mainly heated from below, we continued to focus on studying changes of the cold halocline layer in the monthly mean CMIP5 data.

This study was inspired by observational studies which suggested that the Arctic Ocean cold halocline layer could be become less persistent in a warmer climate, effectively removing "the lid" from the underlying warm Atlantic water (Polyakov et al., 2017; Steele & Boyd, 1998). Our main result is that this suggestion is supported by results from global climate models.

Our analysis suggests that a failure to reduce greenhouse gas emissions would indeed lead to increasingly frequent cold halocline layer thinning events which would facilitate increased energy fluxes from the ocean and can contribute to reducing the sea ice cover. A relatively low salinity of warm water directly below the mixed layer in winter is consistent with the idea that shelf processes play a role (cf, e.g., Timmermans et al., 2018). For most models, the two different algorithms that were used to identify the bottom of the cold halocline and that focus on different characteristics of the cold halocline yield different results regarding the location of the cold halocline bottom. But both algorithms show an increase in the frequency of cold halocline thinning events.

A caveat of this study is the use of monthly mean data from low-resolution global models. Analyzing output from these models is nevertheless interesting and important, since these models contribute to assessment reports such as the Fifth Assessment Report by the Intergovernmental Panel on Climate Change. Unfortunately, the ocean data, which are necessary for this analysis, are only available for a subset of CMIP5 models. Furthermore, only monthly mean output of ocean temperature and salinity has been archived within CMIP5. We are, however, planning to extend our analyses to daily output from shorter runs with a single high-resolution model in the future.

The finding that the suggested increase in the frequency of Arctic cold halocline thinning events in a warmer climate is at least qualitatively reproduced in climate models opens the door for several further studies. Future model studies may (a) help to better quantify the effect that thinning events may have on Arctic warming compared to, for example, the lapse rate feedback and (b) help to better understand the causes of the increased thinning event frequency. In order to better understand the reasons for thinning events to occur, one could, for example, perform trajectory analysis or include idealized tracers in a single model in order to establish the origin of water in the cold halocline. Computing back trajectories would require output at higher temporal resolution.

In today's climate, turbulent vertical mixing of the upper ocean was found to occur in association with tides in the vicinity of sloping or rough surfaces (Rippeth et al., 2015, 2017). It has been hypothesized that turbulent mixing may play a role for the future of the halocline (Giles et al., 2012; Rippeth et al., 2017). Increased turbulent mixing may also play a role in the cold halocline thinning events that are simulated by the CMIP5 models. However, additional model output would be required to determine whether this is indeed the case.

Recently, Polyakov et al. (2018) suggested available potential energy which integrates anomalies of potential density from the surface downward through the surface mixed layer to the base of the halocline as an

alternative indicator for the stability of the cold halocline. Based on this diagnostic, they found a pattern of decreasing stratification in the Eurasian Basin and increasing stratification in the Amerasian Basin for the years 2006–2017 compared to 1981–1995. This pattern resembles the change of the cold halocline depth in the CMIP5 models as diagnosed with the density ratio algorithm (Figure S13b), indicating that this pattern may not be due to internal variability but anthropogenically forced.

Finally, although we presented evidence which, in agreement with suggestions based on existing observations, points to warm water advection and shelf processes as processes that influence the cold halocline, a number of open questions regarding the future of the cold halocline remain. In addition to warming, changes in atmospheric dynamics are expected to affect the cold halocline. As the polar high weakens, onshore winds over the shelf seas weaken which affects the extent of the seasonal ice zones. This could affect the cold halocline in various ways. Further research on this topic is planned using limited area as well as global models in combination with observations.

Acknowledgments
We very much appreciate the insightful comments and constructive suggestions by two anonymous reviewers and by the anonymous reviewers of a shorter previous version of this manuscript. Cornelia Köberle suggested idealized tracers as a means to help determine the origin of water masses in future studies. We thank the climate modeling groups (listed in Table 1) for producing and making available their model output. We acknowledge the World Climate Research Program's Working Group on Coupled Modeling, which is responsible for CMIP. For CMIP the U.S. Department of Energy's Program for Climate Model Diagnosis and Intercomparison provides coordinating support and led development of software infrastructure in partnership with the Global Organization for Earth System Science Portals. The CMIP5 model data that are needed to evaluate the conclusions can be obtained via Earth System Grid Federation servers (e.g., http://pcmdi9.llnl.gov). The NCAR Command Language (Version 6.3.0) [Software] (2015), Boulder, Colorado: UCAR/NCAR/CISL/TDD,_ https://doi.org/10.5065/D6WD3XH5 was used for data visualization. In Figures 9 and 10, Python Matplotlib (Hunter, 2007) version 3.11 (https://doi.org/10.5281/zenodo.3264781) was used. The bathymetry data in Figures 9a and 10a originate from the NOAA ETOPO data set (https://doi.org/10.7289/V5C8276M). We gratefully acknowledge the funding by the Deutsche Forschungsgemeinschaft (DFG, German Research Foundation)—Project-ID 268020496—TRR 172 within the Transregional Collaborative Research Center ArctiC Amplification: Climate Relevant Atmospheric and SurfaCe Processes and Feedback Mechanisms (AC)^3.

References

Aksenov, Y., Bacon, S., Coward, A. C., & George Nurser, A. J. (2010). The North Atlantic inflow to the Arctic Ocean: High-resolution model study. *1–22*, *79*. https://doi.org/10.1016/j.jmarsys.2009.05.003

Arora, V. K., Scinocca, J. F., Boer, G. J., Christian, J. R., Denman, K. L., Flato, G. M., et al. (2011). Carbon emission limits required to satisfy future representative concentration pathways of greenhouse gases. *Geophysical Research Letters*, *38*, L05805. https://doi.org/10.1029/2010GL046270

Årthun, M., Eldevik, L., Smedsrud, L. M., Skakseth, Ø., & Ingvaldsen, R. B. (2012). Quantifying the influence of Atlantic heat on Barents sea ice variability and retreat. *Journal of Climate*, *25*, 4736–4743. https://doi.org/10.1175/JCLI-D-11-00466.1

Bentsen, M., Bethke, I., Debernard, J. B., Iversen, T., Kirkevåg, A., Seland, Ø., et al. (2013). The Norwegian Earth System Model, NorESM1-M—Part 1: Description and basic evaluation of the physical climate. *Geoscientific Model Development*, *6*(3), 687–720. https://doi.org/10.5194/gmd-6-687-2013

Bintanja, R., Graversen, R. G., & Hazeleger, W. (2011). Arctic winter warming amplified by the thermal inversion and consequent low infrared cooling to space. *Nature Geoscience*, *4*, 758–761. https://doi.org/10.1038/NGEO1285

Bintanja, R., & Selten, F. M. (2014). Future increases in Arctic precipitation linked to local evaporation and sea-ice retreat. *Nature*, *509*, 479–482. https://doi.org/10.1038/nature13259

Bourgain, P., & Gascard, J. C. (2011). The Arctic Ocean halocline and its interannual variability from 1997 to 2008. *Deep-Sea Research Part I*, *58*, 745–756. https://doi.org/10.1016/j.dsr.2011.05.001

Burgard, C., & Notz, D. (2017). Drivers of Arctic Ocean warming in CMIP5 models. *Geophysical Research Letters*, *44*, 4263–4271. https://doi.org/10.1002/2016GL072342

Carmack, E. C. (2000). The freshwater budget of the Arctic Ocean: Sources, storage and sinks. *The freshwater budget of the Arctic Ocean*, NATO Adv. Res. Ser. (pp. 91–126). Dordrecht, Netherlands: Kluwer Acad.

Carmack, E. C. (2007). The alpha/beta ocean distinction: A perspective on freshwater fluxes, convection, nutrients and productivity in high-latitude seas. *Deep-Sea Research Part II*, *54*, 2578–2598. https://doi.org/10.1016/j.dsr2.2007.08.018

Carmack, E., Polyakov, I., Padman, L., Fer, I., Hunke, E., Hutchings, J., & Winsor, P. (2015). Toward quantifying the increasing role of oceanic heat in sea ice loss in the new Arctic. *Bulletin of the American Meteorological Society*, *96*, 2079–2105. https://doi.org/0.1175/BAMS-D-13-00177.1

Carmack, E. C., Yamamoto-Kawai, M., Haine, T. W. N., Bacon, S., Bluhm, B. A., Lique, C., & Williams, W. J. (2016). Freshwater and its role in the Arctic marine system: Sources, disposition, storage, export, and physical and biogeochemical consequences in the Arctic and global oceans. *Journal of Geophysical Research: Biogeosciences*, *121*, 675–717. https://doi.org/10.1002/2015JG003140

Cohen, J., Screen, J. A., Furtado, J. C., Barlow, M., Whittleston, D., Coumou, D., et al. (2014). Recent Arctic amplification and extreme mid-latitude weather. *Nature Geoscience*, *7*, 627–637. https://doi.org/10.1038/NGEO2234

Donner, L. J., Wyman, B. L., Hemler, R. S., Horowitz, L. W., Ming, Y., Zhao, M., et al. (2011). The dynamical core, physical parameterizations, and basic simulation characteristics of the atmospheric component AM3 of the GFDL global coupled model CM3. *Journal of Climate*, *24*(13), 3484–3519. https://doi.org/10.1175/2011JCLI3955.1

Dufresne, J.-L., Foujols, M.-A., Denvil, S., Caubel, A., Marti, O., Aumont, O., & Vuichard, N. (2013). Climate change projections using the IPSL-CM5 Earth System Model: from CMIP3 to CMIP5. *Climate Dynamics*, *40*, 2123–2165. https://doi.org/10.1007/s00382-012-1636-1

Dunne, J. P., Jasmin, J. G. J., Adcroft, A. J., Griffies, S. M., Hallberg, R. W., Shevliakova, E., et al. (2012). GFDLs ESM2 global coupled climate-carbon earth system models. Part I: Physical formulation and baseline simulation characteristics. *Journal of Climate*, *25*(19), 6646–6665. https://doi.org/10.1175/JCLI-D-11-00560.1

Gent, P. R., Danabasoglu, G., Donner, L. J., Holland, M. M., Hunke, E. C., Jayne, S. R., et al. (2011). The Community Climate System Model Version 4. *Journal of Climate*, *24*(19), 4973–4991. https://doi.org/10.1175/2011JCLI4083.1

Giles, K. A., Laxon, S. W., Ridout, A. L., Wingham, D. J., & Bacon, S. (2012). Western Arctic Ocean freshwater storage increased by wind-driven spin-up of the Beaufort Gyre. *Nature Geoscience*, *5*, 194–197. https://doi.org/10.1038/NGEO1379

Gill, A. E. (1982). *Atmosphere-ocean dynamics*. New York, NY: Academic Press.

Giorgetta, M. A., Jungclaus, J., Reick, C. H., Legutke, S., Bader, J., Böttinger, M., et al. (2013). Climate and carbon cycle changes from 1850 to 2100 in MPI-ESM simulations for the Coupled Model Intercomparison Project phase 5. *Journal of Advances in Modeling Earth Systems*, *5*, 572–597. https://doi.org/10.1002/jame.20038

Haine, T. W. N., Curry, B., Gerdes, R., Hansend, E., Karcher, M., Lee, C., et al. (2015). Arctic freshwater export: Status, mechanisms, and prospects. *Global and Planetary Change*, *125*, 13–35. https://doi.org/10.1016/j.gloplacha.2014.11.013

Hunter, J. D. (2007). Matplotlib: A 2D graphics environment. *Computing in Science & Engineering*, *9*(3), 90–95. https://doi.org/10.1109/MCSE.2007.55

Itkin, P., Losch, M., & Gerdes, R. (2015). Landfast ice affects the stability of the Arctic halocline: Evidence from a numerical model. *Journal of Geophysical Research: Oceans*, *120*, 2622–2635. https://doi.org/10.1002/2014JC010353

Joshi, M., Shine, K., Ponater, M., Stuber, N., Sausen, R., & Li, L. (2003). A comparison of climate response to different radiative forcings in three general circulation models: Towards an improved metric of climate change. *Climate Dynamics*, *20*, 843–854. https://doi.org/10.1007/s00382-003-0305-9

Laîné, A., Yoshimori, M., & Abe-Ouchi, A. (2016). Surface Arctic amplification factors in CMIP5 models: Land and oceanic surfaces and seasonality. *Journal of Climate*, *29*(9), 3297–3316. https://doi.org/10.1175/JCLI-D-15-0497.1

Manabe, S., & Wetherald, R. T. (1975). The effects of doubling the CO_2 concentration on the climate of a general circulation model. *Journal of the Atmospheric Sciences*, *32*, 3–15. https://doi.org/10.1175/1520-0469(1975)032<0003:TEODTC>2.0.CO;2

Martin, G. M., Bellouin, N., Collins, W., Culverwell, I. D., Halloran, P. R., Hardiman, S. C., et al. (2011). The HadGEM2 family of Met Office Unified Model climate configurations. *Geoscientific Model Development*, *4*(3), 723–757. https://doi.org/10.5194/gmd-4-723-2011

Maykut, G. A., & Untersteiner, N. (1971). Some results from a time-dependent thermodynamic model of sea ice. *Journal of Geophysical Research*, *76*(6), 1550–1575. https://doi.org/10.1029/JC076i006p01550

Newton, J. L., & Coachman, L. K. (1974). Atlantic water circulation in the Canada Basin. *Arctic*, *27*, 297–303.

Nummelin, A., Li, C., & Hezel, P. J. (2017). Connecting ocean heat transport changes from the midlatitudes to the Arctic Ocean. *Geophysical Research Letters*, *44*, 1899–1908. https://doi.org/10.1002/2016GL071333

Peralta-Ferriz, C., & Woodgate, R. A. (2015). Seasonal and interannual variability of pan-Arctic surface mixed layer properties from 1979 to 2012 from hydrographic data, and the dominance of stratification for multiyear mixed layer depth shoaling. *Progress in Oceanography*, *134*, 19–53. https://doi.org/10.1016/j.pocean.2014.12.005

Pithan, F., & Mauritsen, T. (2014). Arctic amplification dominated by temperature feedbacks in contemporary climate models. *Nature Geoscience*, *7*(3), 181–184. https://doi.org/10.1038/NGEO2071

Polyakov, I. V., Pnyushkov, A. V., Alkire, M. B., Ashik, I. M., Baumann, T. M., Carmack, E. C., et al. (2017). Greater role for Atlantic inflows on sea-ice loss in the Eurasian Basin of the Arctic Ocean. *Science*, *356*, 285–291. https://doi.org/10.1126/science.aai8204

Polyakov, I. V., Pnyushkov, A. V., & Carmack, E. C. (2018). Stability of the Arctic halocline: A new indicator of Arctic climate change. *Environmental Research Letters*, *13*, 125008. https://doi.org/10.1088/1748-9326/aaec1e

Polyakov, I. V., Timokhov, L., Alexeev, V. A., Bacon, S., Dmitrenko, I. A., Fortier, L., et al. (2010). Arctic Ocean warming contributes to reduced polar ice cap. *Journal of Physical Oceanography*, *40*, 2743–2756.

Rippeth, T. P., Lincoln, B. J., Lenn, Y.-D., Mattias Green, J. A., Sundfjord, A., & Bacon, S. (2015). Tide-mediated warming of Arctic halocline by Atlantic heat fluxes over rough topography. *Nature Geoscience*, *8*, 191–194. https://doi.org/10.1038/NGEO2350

Rippeth, T. P., Vlasenko, V., Stashchuk, N., Scannell, B. D., Green, J. A. M., Lincoln, B. J., & Bacon, S. (2017). Tidal conversion and mixing poleward of the critical latitude (an Arctic case study). *Geophysical Research Letters*, *44*, 12,349–12,357. https://doi.org/10.1002/2017GL075310

Rotstayn, L. D., Jeffrey, S. J., Collier, M. A., Dravitzki, S. M., Hirst, A. C., Syktus, J. I., & Wong, K. K. (2012). Aerosol- and greenhouse gas-induced changes in summer rainfall and circulation in the Australasian region: A study using single-forcing climate simulations. *Atmospheric Chemistry and Physics*, *12*(14), 6377–6404. https://doi.org/10.5194/acp-12-6377-2012

Rudels, B., Jones, E. P., Anderson, L. G., & Kattner, G. (1994). On the intermediate depth waters of the Arctic Ocean. *The Polar Oceans and their role in shaping the global environment* (pp. 33–46). Washington, DC: American Geophysical Union. https://doi.org/10.1029/GM085p0033

Salzmann, M. (2017). The polar amplification asymmetry: Role of Antarctic surface height. *Earth System Dynamics*, *8*, 323–336. https://doi.org/10.5194/esd-8-323-2017

Schmidt, G. A., Kelley, M., Nazarenko, L., Ruedy, R., Russell, G. L., Aleinov, I., et al. (2014). Configuration and assessment of the GISS ModelE2 contributions to the CMIP5 archive. *Journal of Advances in Modeling Earth Systems*, *6*, 141–184. https://doi.org/10.1002/2013MS000265

Screen, J. A., & Simmonds, I. (2010a). The central role of diminishing sea ice in recent Arctic temperature amplification. *Nature*, *464*, 1334–1337. https://doi.org/10.1038/nature09051

Screen, J. A., & Simmonds, I. (2010b). Increasing fall winter energy loss from the Arctic Ocean and its role in Arctic temperature amplification. *Journal of Geophysical Research*, *37*, L16707. https://doi.org/10.1029/2010GL044136

Serreze, M. C., Barrett, A. P., Stroeve, J. C., Kindig, D. N., & Holland, M. M. (2009). The emergence of surface-based Arctic amplification. *Cryosphere*, *3*, 11–19. https://doi.org/10.5194/tc-3.11-2009

Spielhagen, R. F., Werner, K., Sørensen, S. A., Zamelczyk, K., Kandiano, E., Budeus, G., et al. (2011). Enhanced modern heat transfer to the Arctic by warm Atlantic water. *Science*, *331*, 450–453. https://doi.org/10.1126/science.1197397

Steele, M., & Boyd, T. (1998). Retreat of the cold halocline layer in the Arctic Ocean. *Journal of Geophysical Research*, *103*, 10,419–10,435. https://doi.org/10.1029/98JC00580

Taylor, K. E., Stouffer, R. J., & Meehl, G. A. (2012). An overview of CMIP5 and the experiment design. *Bulletin of the American Meteorological Society*, *93*(4), 485–498. https://doi.org/10.1175/BAMS-D-11-00094.1

Timmermans, M.-L., Toole, J., & Krishfield, R. (2018). Warming of the interior Arctic Ocean linked to sea ice losses at the basin margins. *Science Advances*, *4*, eaat6773. https://doi.org/10.1126/sciadv.aat6773

Voldoire, A., Sanchez-Gomez, E., Salas y Mélia, D., Decharme, B., Cassou, C., Sénési, S., et al. (2013). The CNRM-CM5.1 global climate model: Description and basic evaluation. *Climate Dynamics*, *40*(9-10), 2091–2121. https://doi.org/10.1007/s00382-011-1259-y

Watanabe, S., Hajima, T., Sudo, K., Nagashima, T., Takemura, T., Okajima, H., et al. (2011). MIROC-ESM 2010: Model description and basic results of CMIP5-20c3 m experiments. *Geoscientific Model Development*, *4*(4), 845–872. https://doi.org/10.5194/gmd-4-845-2011

Woodgate, R. A. (2018). Increases in the Pacific inflow to the Arctic from 1990 to 2015, and insights into seasonal trends and driving mechanisms from year-round Bering Strait mooring data. *Progress in Oceanography*, *160*, 124–154. https://doi.org/10.1016/j.pocean.2017.12.007

Yang, X.-Y., Fyfe, J. C., & Flato, G. M. (2010). The role of poleward energy transport in Arctic temperature evolution. *Geophysical Research Letters*, *37*, L14803. https://doi.org/10.1029/2010GL043934

Yukimoto, S., Adachi, Y., Hosaka, M., Sakami, T., Yoshimura, H., Hirabara, M., et al. (2012). A new global climate model of the Meteorological Research Institute: MRI-CGCM3—Model description and basic performance. *Journal of the Meteorological Society of Japan*, *90A*, 23–64. https://doi.org/10.2151/jmsj.2012-A02

Zhang, X., He, J., J. Zhang, J. I. P., Gerdes, R., & Wu, P. (2013). Enhanced poleward moisture transport and amplified northern high-latitude wetting trend. *Nature Climate Change*, *3*, 47–51. https://doi.org/10.1038/NCLIMATE1631